Chinese Chemical Letters 36 (2025) 109999

Contents lists available at ScienceDirect

Chinese Chemical Letters

journal homepage: www.elsevier.com/locate/cclet

Supramolecular prodrug vesicles for selective antimicrobial therapy employing a chemo-photodynamic strategy

Hao Sun[a,1], Shengke Li[b,1,*], Qian Liu[a], Minzan Zuo[a], Xueqi Tian[a], Kaiya Wang[a,*], Xiao-Yu Hu[a,c,*]

[a] College of Materials Science and Technology, Nanjing University of Aeronautics and Astronautics, Nanjing 211106, China
[b] Macao Centre for Research and Development in Chinese Medicine, Institute of Chinese Medical Sciences, University of Macau, Macau 999078, China
[c] Qinghai Provincial Key Laboratory of Tibetan Medicine Research and Key Laboratory of Tibetan Medicine Research, Northwest Institute of Plateau Biology, Chinese Academy of Sciences, Xining 810008, China

ARTICLE INFO

Article history:
Received 1 March 2024
Revised 29 April 2024
Accepted 10 May 2024
Available online 11 May 2024

Keywords:
Supramolecular prodrug
Selective antibacterial activity
Host-guest complex
Cavitand
Combination therapy

ABSTRACT

Supramolecular prodrug vesicles (**H-4**⊃**B-2**@MB) with selective antibacterial activity have been successfully constructed. Specifically, a natural antibiotic prodrug (**B-2**) with glutathione (GSH)-responsiveness was synthesized. The hydrophobic interaction between **B-2** and a novel water-soluble cavitand with deep cavity (**H-4**) resulted in the formation of a host-guest complex, which further self-assembled into supramolecular vesicles. The formed vesicles could effectively encapsulate the photosensitizer methylene blue (MB), enabling co-delivery of antibiotics and photosensitizers in the presence of GSH. Moreover, upon excitation at 630 nm, the photosensitizers generate reactive oxygen species (ROS), effectively eradicating *E. coli* through combined chemo-photodynamic therapy. Considering that GSH is predominantly present in Gram-negative bacteria such as *E. coli*, this strategy exhibits substantial potential for selectively inhibiting bacteria characterized by high GSH levels to regulate bacterial colony equilibrium.

The prevention and control of bacterial infections are pivotal and challenging issues in global public health [1,2]. Antibiotics can inhibit or kill bacteria in the human body, which have saved countless individuals from diverse bacterial infections [3-5]. However, the rapid evolution of antibiotic resistance, caused by the rampant overuse and misuse of these drugs, can significantly reduce treatment efficacy and disrupt bacterial colony balance at infection sites within a short period of time [6,7]. To avoid overuse of antibiotics and obtain more effective antimicrobials, combination therapy is deemed as one of the most promising strategies owing to its ability to meet the multiple requirements of pathogen microenvironment [8,9]. Combination therapy refers to the conjunction of different types of drugs or remedies (*e.g.*, chemotherapy and radiotherapy, chemodynamic therapy and photodynamic therapy (PDT), chemotherapy and PDT) to increase the ability of killing pathogens and improving the lives of patients [10-12]. PDT transfers the energy of light to the surrounding oxygen molecules *via* photosensitizers, thereby generating reactive oxygen species (ROS) to kill pathogens [13,14]. It is worth noting that PDT does not lead to drug resistance, and no toxicity will be caused by drug accumulation [15]. Therefore, PDT based combination therapy strategies have attracted increasing attention [16,17]. Although impressive results have been achieved by these remedies, it is still crucial to develop novel combination therapy strategies that exhibit excellent strain-selectivity toward various bacteria [18-20].

Due to the rapid development of macrocyclic chemistry [21-23], strategies for the diagnosis and treatment of diseases based on supramolecular assembly have sprung up [24-26]. Among them, host-guest complex-based prodrug delivery systems have garnered increasing attention owing to their responsiveness to external stimuli and high drug loading efficiency [27,28], which makes prodrug strategies competitive for targeted and selective therapy of pathogens. Furthermore, incorporating drugs or photosensitizers into supramolecular prodrugs offers a promising avenue for combination therapy, thereby potentially enhancing the efficacy of targeted therapeutic interventions.

In this paper, we present a chemo-photodynamic antimicrobial strategy based on supramolecular prodrug vesicles for inhibiting bacteria with high concentrations of glutathione (GSH) (Scheme 1). Specifically, a new cavitand (**H-4**) with a hydrophilic surface and a hydrophobic deep cavity was successfully synthesized. The pos-

* Corresponding authors.
E-mail addresses: walterli@um.edu.mo (S. Li), kwang6@nuaa.edu.cn (K. Wang), huxy@nuaa.edu.cn (X.-Y. Hu).
[1] These authors contributed equally to this work.

https://doi.org/10.1016/j.cclet.2024.109999
1001-8417/

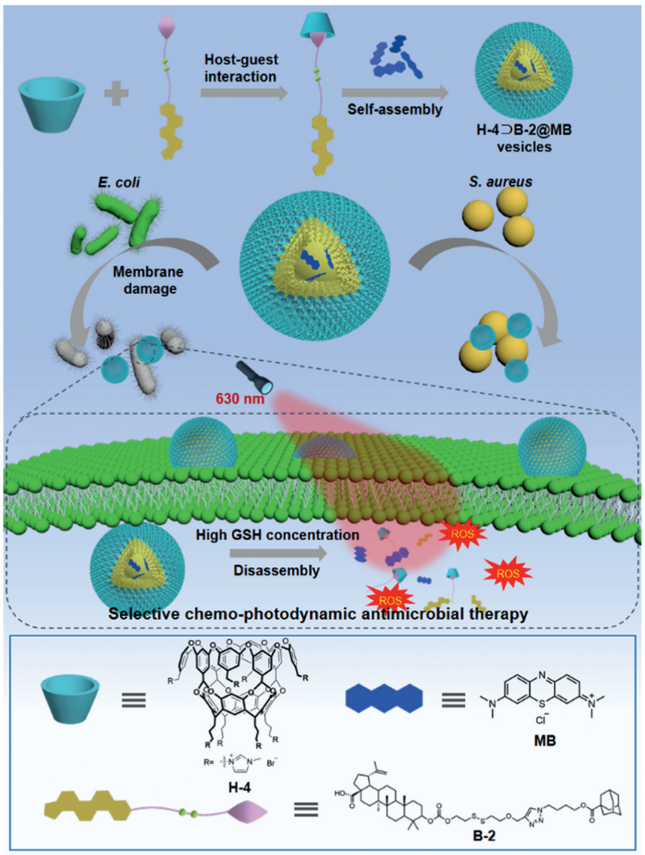

Scheme 1. Illustration of the formation of supramolecular prodrug vesicles and their selective chemo-photodynamic antimicrobial process.

itive charges on the surface of **H-4** facilitate its strong binding to negatively charged bacterial cell membranes, resulting in the disruption of membrane structure and integrity through electrostatic adsorption. Consequently, bacterial activity is effectively inhibited. Additionally, the hydrophobic deep cavity of **H-4** allowed for accommodation of various types of guest molecules [29]. Betulinic acid, a natural hydrophobic antibiotic [30], was co-modified into prodrug guests (**B-2**) by incorporating an adamantane moiety and a disulfide bond. These modifications significantly improved its bioavailability and binding affinity with **H-4**, and more importantly endowed it with GSH-responsive capability [31]. Through host-guest interactions between **H-4** and **B-2**, prodrug amphiphiles were formed and further assembled into supramolecular prodrug vesicles (**H-4⊃B-2**) in aqueous solution. By encapsulating methylene blue (MB) within the cavity of **H-4⊃B-2** vesicles, photosensitizer-loaded prodrug vesicles (**H-4⊃B-2**@MB) were successfully prepared. Endocytosis facilitated the successful internalization of **H-4⊃B-2**@MB vesicles into *E. coli*. Within the cytoplasm of *E. coli*, a relatively high concentration of GSH cleaved the disulfide bond present in **B-2**, leading to effective disassembly of **H-4⊃B-2**@MB vesicles and subsequent co-release of antibiotics and photosensitizers from their encapsulation sites. Meanwhile, upon excitation at 630 nm, photosensitizers generated ROS, effectively eradicating bacteria *via* combined chemo-photodynamic therapy. Therefore, the targeted suppression of bacteria with high GSH content can be achieved using **H-4⊃B-2**@MB prodrug vesicles. Considering that GSH is particularly abundant in Gram-negative bacteria like *E. coli* [32], this approach holds great potential for developing Gram-selective antibacterial strategies aimed at regulating bacterial colony balance in future clinical treatment.

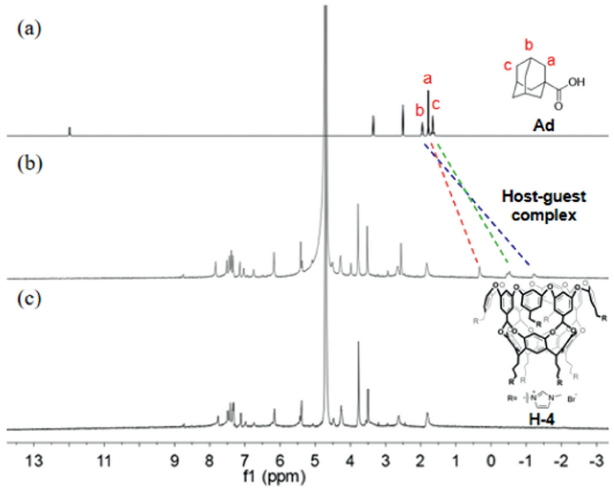

Fig. 1. ^{1}H NMR spectra (400 MHz, D_2O, 298 K) of (a) Ad (1.0 mmol/L), (b) Host-guest complex (**H-4**:Ad = 1:1) and (c) **H-4** (1.0 mmol/L).

H-4 and **B-2** were synthesized according to the reported procedure [33-35], respectively (Schemes S1 and S2 in Supporting information). Their chemical structures were characterized by ^{1}H NMR, ^{13}C NMR, ^{1}H–^{1}H COSY, HR-MS (Figs. S1–S14 in Supporting information). Initially, to avoid complicated assembly, the binding behavior of **H-4** and **B-2** was studied using 1-adamantane carboxylic acid (Ad) as a model guest in D_2O. ^{1}H NMR spectra (Fig. 1) of host-guest complex showed that the proton signals of Ad exhibited a prominent upfield chemical shift by the inclusion-induced shielding effect. The stoichiometry between **H-4** and **B-2** was 1:1 as measured by the Job's plot method through UV–vis spectroscopy (Fig. S15 in Supporting information). An obvious Tyndall effect was observed after the addition of **B-2** into an aqueous solution of **H-4** (Fig. S16 in Supporting information), indicating that a large number of nanoparticles were formed. Furthermore, the best molar ratio for **B-2** and **H-4** to form nanoaggregates in water was 6:1 as determined by UV–vis transmittance at 500 nm (Fig. S17 in Supporting information). Based on the above-mentioned molar ratio, the critical aggregation concentration value was determined to be 2.14×10^{-5} mol/L (Fig. S18 in Supporting information). After encapsulating MB into the cavity of **H-4⊃B-2** vesicles, we successfully prepared supramolecular prodrug vesicles loaded with the photosensitizer **H-4⊃B-2**@MB, which showed obvious Tyndall effect (Fig 2a). The morphology and size of **H-4⊃B-2**@MB assemblies were characterized by scanning electron microscope (SEM), transmission electron microscope (TEM) and dynamic light scattering (DLS), respectively. The SEM image and TEM image confirmed the hollow vesicle formation of **H-4⊃B-2**@MB and the vesicles had a regular shape with an estimated diameter of ~200 nm (Figs. 2b and c), which was consistent with the hydrodynamic diameter (220 nm) as measured by DLS (Fig. 2d). Zeta-potential (19.4 mV) of the **H-4⊃B-2**@MB vesicle originated from the positively charged macrocycle host, confirming its good stability in solution (Fig. S20 in Supporting information). All detailed procedures for the fabrication of **H-4⊃B-2**@MB vesicles were shown in Supporting information.

The disulfide bond in **B-2** is sensitive to GSH, therefore **H-4⊃B-2**@MB vesicles should possess GSH-responsiveness. As shown in Fig. 3a, after **H-4⊃B-2**@MB vesicles being incubated with GSH (5.0 mmol/L, close to GSH concentration in *E. coli* cytoplasm [36]) for 0.5 h, the fluorescent intensity at 690 nm corresponding to MB emission increased gradually along with incubation time, indicating the successful release of encapsulated MB. On the contrary, **H-4⊃B-2**@MB vesicles showed almost no significant changes in fluorescence intensity after being incubated in water for over

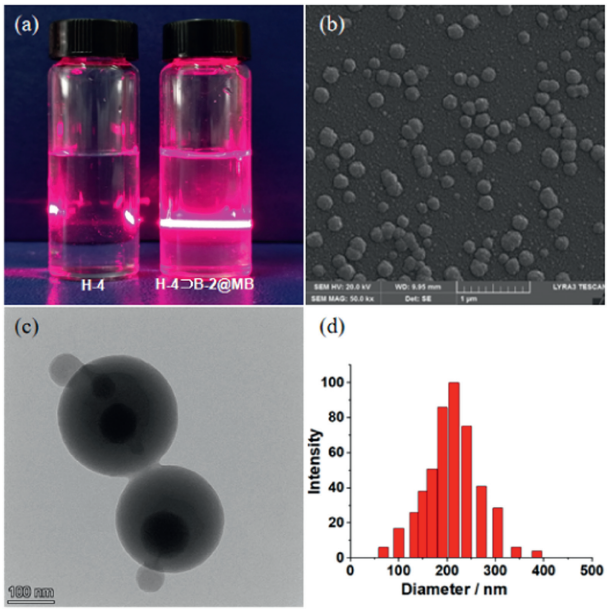

Fig. 2. (a) Tyndall effect, (b) SEM image, (c) TEM image, and (d) DLS size distribution of **H-4⊃B-2**@MB vesicles, respectively.

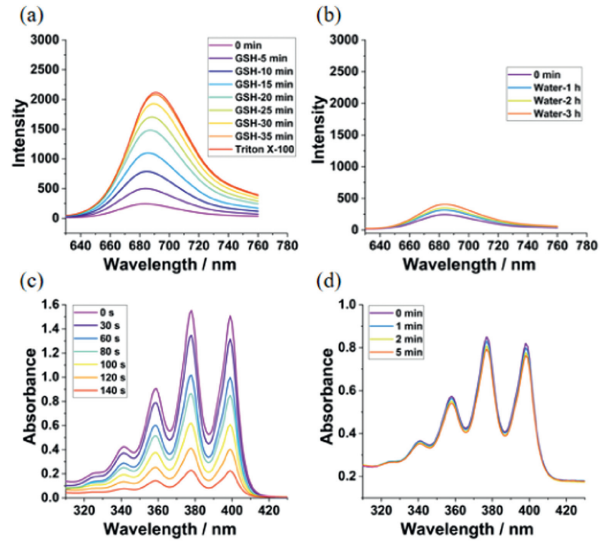

Fig. 3. Fluorescence spectra of **H-4⊃B-2**@MB vesicles after being incubated with (a) GSH and Triton X-100, and (b) water for different time periods; Absorption spectra of ABDA in the presence of **H-4⊃B-2**@MB vesicles after being incubated with (c) GSH (C_{GSH} = 5.0 mmol/L, t = 40 min) and (d) with water (t = 40 min) under different time periods with light (630 nm, 20 mW/cm^2). [**H-4⊃B-2**@MB] = 0.10 mmol/L, [ABDA] = 0.10 mmol/L.

3 h (Fig. 3b). To rule out the possibility that fluctuations in fluorescence signals were caused by time-dependent instability of the vesicles themselves or non-specific factors, we conducted extended incubation experiments under various conditions, including different temperatures and pH levels. Throughout these experiments, changes in fluorescence intensity were continuously monitored. The results indicate that, apart from GSH, no other potential factors significantly influenced the observed signal variations (Fig. S21 in Supporting information). Disulfide bonds, as the stimulus-responsive element in a prodrug, can be efficiently cleaved under high concentrations of GSH. The guest molecule **B-2** is covalently linked to betulinic acid through disulfide bonds with adamantane units. When exposed to high concentrations of GSH, the disulfide bond within the **B-2** molecule undergoes specific cleavage by GSH, thereby releasing the betulinic acid moiety and photosensitizers into the surrounding environment. This cleavage process not only facilitates effective release of the therapeutic agent but also triggers structural changes within the vesicle itself, reducing its stability and ultimately leading to vesicle disassembly. The Tyndall effect of the vesicle solution before and after incubation with GSH (Fig. S22 in Supporting information) further corroborates this conclusion. This feature enables **H-4⊃B-2@**MB vesicles to effectively target and treat pathogens with high GSH concentration.

Since PDT efficacy is closely related to the ROS generation ability of photosensitizers, a ROS indicator 9,10-anthracenediyl-bis(methylene)dimalonic acid (ABDA) was employed to confirm the ROS generation by the disassembled **H-4⊃B-2**@MB vesicles. The UV absorbance of ABDA at 400 nm significantly decreased upon irradiation with 630 nm light in GSH-incubated **H-4⊃B-2**@MB vesicles, which can be attributed to the reaction between ABDA and ROS generated by MB (Fig. 3c). The gradual decrease in absorbance of ABDA with increasing light irradiation time indicates continuous generation of ROS. Therefore, it is expected that upon excitation at 630 nm, the **H-4⊃B-2**@MB vesicles can achieve an increased concentration of local ROS, leading to enhanced cytotoxicity for chemo-photodynamic therapy. In contrast to GSH-incubated **H-4⊃B-2**@MB vesicles, water-incubated **H-4⊃B-2**@MB vesicles showed a negligible decrease in UV absorption in the presence of ABDA under 630 nm light irradiation (Fig. 3d).

After confirming the GSH-responsiveness and photodynamic therapy ability, *E. coli* and *S. aureus*, as representatives of two different common pathogenic bacteria, were used to evaluate the antibacterial efficacy of **H-4⊃B-2**@MB in the presence or absence of 630 nm light irradiation. As shown in Figs. 4a and c, **H-4⊃B-2** and **H-4⊃B-2**@MB exhibited certain antibacterial activity against *E. coli* at a concentration of 2 μmol/L under dark conditions, and the antibacterial activity of **H-4⊃B-2**@MB was remarkably enhanced upon 630 nm light irradiation, resulting in about 70% reduction of colony-forming unit (CFU) ratio.

When the concentration was increased to 10.0 μmol/L, the antibacterial activity of **H-4⊃B-2** and **H-4⊃B-2**@MB was further enhanced, exhibiting a 99% reduction in CFU ratio of *E. coli* upon exposure to 630 nm light in the **H-4⊃B-2**@MB group. Moreover, CFU reduction rate of **H-4⊃B-2**@MB was increased along with light irradiation time (Fig. S24 in Supporting information), suggesting an irradiation time dependent antibacterial activity of **H-4⊃B-2**@MB, which is presumably due to the sustained ROS generation of MB. The tolerance of *S. aureus* treated with the same concentration of **H-4⊃B-2** and **H-4⊃B-2**@MB (10.0 μmol/L) was superior to that of *E. coli* under dark conditions (Fig. 4b and d). Even after exposure to 630 nm light treatment, the CUF ratio of *S. aureus* remained above 50%. The presence of MB did not improve the antibacterial activity of **H-4⊃B-2**@MB against *S. aureus* upon 630 nm light irradiation, indicating that MB did not contribute to the inhibition of *S. aureus.*

The observed circumstances can be attributed to the disparity in GSH concentrations within the two bacterial species. The enhanced antibacterial activity of supramolecular prodrug vesicles against *E. coli* can be ascribed to the millimolar GSH concentration in its cytoplasm, which is necessary for the disassembly of vesicles and subsequent release of antibiotic betulinic acid and photosensitizer MB. In contrast, the absence of GSH in Gram-positive bacteria such as *S. aureus* impedes the disassembly of **H-4⊃B-2**@MB vesicles, hindering their antibacterial and PDT effects. In summary, this study demonstrates that **H-4⊃B-2**@MB has the ability to selectively inhibit bacteria with high concentrations of GSH.

To verify whether the significantly enhanced antibacterial effect upon 630 nm light irradiation was due to ROS generation, 2,7-dichlorofluorescein diacetate (DCFH-DA), which can be transformed into 2,7-dichlorofluorescein (DCF) with strong green fluorescence when reacts with ROS, was used as a ROS probe. Confocal laser

scanning microscope (CLSM) images of *E. coli* treated with DCFH-DA were shown in Fig. S24. *E. coli* treated with **H-4⊃B-2**@MB vesicles exhibited strong green fluorescence upon exposure to 630 nm light, indicating *in situ* ROS generation of the released MB from **H-4⊃B-2**@MB vesicles. However, negligible fluorescence was observed for both control group and **H-4⊃B-2**@MB vesicles without light irradiation. This suggests that the antibacterial activity can be enhanced by the generated ROS under 630 nm light irradiation. To acquire further details of antibacterial activity of **H-4⊃B-2**@MB against *E. coli* in both dark and under 630 nm light irradiation, SEM was employed to catch the morphological changes of bacteria. In the control group treated with Luria-Bertani (LB) broth, smooth surfaces and intact structure of bacterial cells were observed, indicating that the light exhibited negligible effect on bacterial activity (Figs. 5a and b). For **H-4⊃B-2**@MB-treated *E. coli* in the dark, sectionally damaged membranes were observed (Fig. 5c). This result can be attributed to the combined action of antibiotic betulinic acid and positively charged water-soluble host. Upon 630 nm light irradiation, fragmented bacterial cells were observed in **H-4⊃B-2**@MB-treated *E. coli* group, with some completely collapsing due to the generation of ROS from the released MB photosensitizers (Fig. 5d).

In conclusion, we have successfully constructed GSH-responsive supramolecular prodrug vesicles **H-4⊃B-2**@MB for selective inhibition of bacteria with high concentrations of GSH *via* combined chemo-photodynamic therapy. *In vitro* studies demonstrated that **H-4⊃B-2**@MB vesicles could achieve efficient delivery and selective release of antibiotics and photosensitizers triggered by GSH stimulation. This system exhibits high ROS production, exceptional selectivity, and excellent bacteriostatic effects against *E. coli*. The present study presents a straightforward and effective therapeutic approach with long-lasting implications for combating bacterial infections and facilitating selective treatment. Specifically, by replacing MB with NIR-responsive or ultrasound-responsive sensitizer, it offers a novel avenue for enhanced tissue penetration in photodynamic therapy.

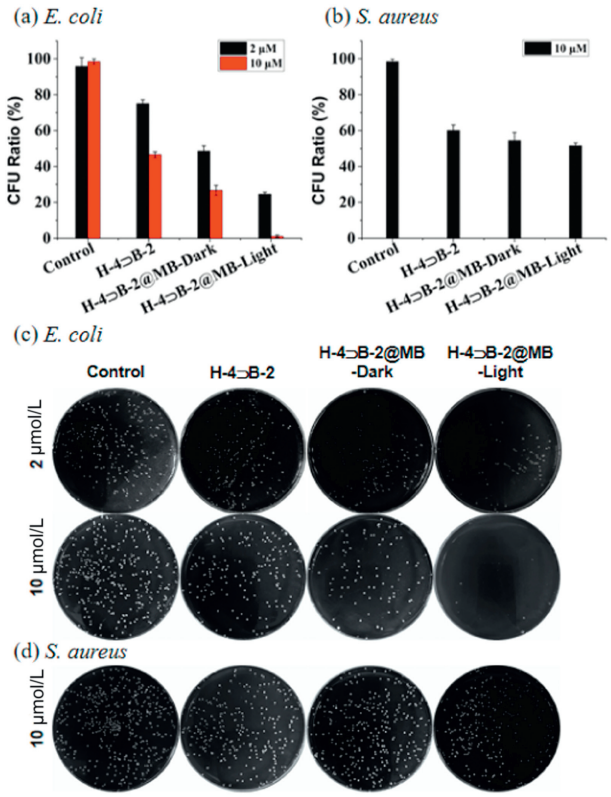

Fig. 4. (a, b) CFU rates and (c, d) representative CFU on LB agar plate for *E. coli* and *S. aureus*, after incubated with different concentrations of **H-4⊃B-2** and **H-4⊃B-2**@MB in dark and light (630 nm, 120 s). Note: Standard deviations (SD) were calculated for $n = 3$. In (a), the mean values showed a significant difference from the control group at $P < 0.05$; in (b), the mean values did not show a significant difference from the control group at $P > 0.05$, as determined by one-way ANOVA. μM: μmol/L.

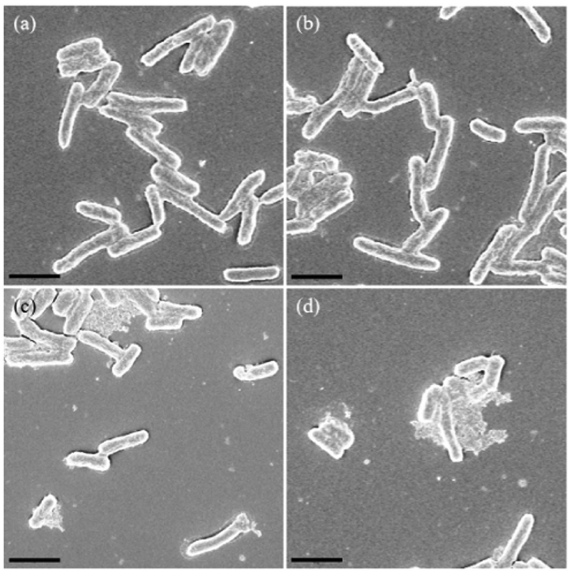

Fig. 5. Morphologies of *E. coli* treated with LB (a) in the dark, (b) under 630 nm light, and with **H-4⊃B-2**@MB vesicles (c) in the dark, and (d) under 630 nm light. Scale bar: 2 μm.

Declaration of competing interest

The authors declare that they have no known competing financial interests or personal relationships that could have appeared to influence the work reported in this paper.

CRediT authorship contribution statement

Hao Sun: Writing – original draft, Methodology, Investigation. **Shengke Li:** Writing – review & editing, Methodology, Investigation. **Qian Liu:** Investigation. **Minzan Zuo:** Investigation. **Xueqi Tian:** Investigation. **Kaiya Wang:** Writing – review & editing, Supervision, Methodology, Funding acquisition. **Xiao-Yu Hu:** Writing – review & editing, Supervision, Project administration, Methodology, Funding acquisition.

Acknowledgments

This work was supported by the National Natural Science Foundation of China (No. 22271154), Natural Science Foundation of Jiangsu Province (No. BK20211179), Innovation Support Program of Jiangsu Province (No. BZ2023055), Fundamental Research Funds for the Central Universities (No. NS2023033), China Postdoctoral Science Foundation (No. 2023M731658), and Achievement Transformation Project of Qinghai Province (No. 2021-SF-145).

Supplementary materials

Supplementary material associated with this article can be found, in the online version, at doi:10.1016/j.cclet.2024.109999.

References

[1] F. Li, M. Zang, S. Liu, et al., J. Mater. Chem. B 9 (2021) 2066–2072.
[2] D. He, Y. Tan, P. Li, et al., Chin. Chem. Lett. 32 (2021) 1743–1746.
[3] V.-N. Nguyen, Z. Zhao, B.Z. Tang, et al., Chem. Soc. Rev. 51 (2022) 3324–3340.
[4] Y. Zhao, L. Chen, Y. Wang, et al., Nano Res. 14 (2021) 4417–4441.
[5] X. Tian, S. Li, K. Velmurugan, et al., Mater. Chem. Front. 7 (2023) 2484–2492.
[6] M.M.S. Lee, E.Y. Yu, D. Yan, et al., ACS Nano 17 (2023) 17004–17020.
[7] X. Zhang, X. Chen, Y. Guo, et al., Angew. Chem. Int. Ed. 60 (2021) 14013–14021.
[8] X. Hu, H. Zhang, Y. Wang, et al., Chem. Eng. J. 450 (2022) 138129.
[9] R. Bholakant, B. Dong, X. Zhou, et al., J. Mater. Chem. B 9 (2021) 8718–8738.
[10] D. Lee, J. Shin, H. Son, et al., Nanoscale Adv. 5 (2023) 1600–1610.
[11] J. Xu, Y. Lai, F. Wang, et al., Chin. Chem. Lett. 34 (2023) 108332.
[12] R. Wu, H. Wang, L. Hai, et al., Chin. Chem. Lett. 31 (2020) 189–192.
[13] K. Liu, Y. Liu, Y. Yao, et al., Angew. Chem. Int. Ed. 52 (2013) 8285–8289.
[14] M. Piksa, C. Lian, I.C. Samuel, et al., Chem. Soc. Rev. 52 (2023) 1697–1722.
[15] J. Xie, Y. Wang, W. Choi, et al., Chem. Soc. Rev. 50 (2021) 9152–9201.
[16] M. Overchuk, R.A. Weersink, B.C. Wilson, et al., ACS Nano 17 (2023) 7979–8003.
[17] B. Li, W. Wang, L. Zhao, et al., ACS Nano 17 (2023) 4601–4618.
[18] Y. Yang, P. He, Y. Wang, et al., Angew. Chem. Int. Ed. 56 (2017) 16239–16242.
[19] D. Lee, L. Dong, Y. Kim, et al., Adv. Healthc. Mater. 12 (2023) 2203136.
[20] X. Huang, C. Lu, W. Zhang, et al., ACS Nano 17 (2023) 14893–14903.
[21] K. Wang, Q. Liu, L. Zhou, et al., Chin. Chem. Lett. 34 (2023) 108559.
[22] K. Wang, R. Zhang, Z. Song, et al., Adv. Sci. 10 (2023) 2206897.
[23] T. Zhang, K. Wang, X. Huang, et al., Chem. Eur. J. 29 (2023) e202203738.
[24] Y. Zhou, H. Tang, H. Wu, et al., Chin. Chem. Lett. 35 (2024) 108626.
[25] S. Li, J.J. Li, Y.Y. Zhao, et al., ACS Nano 17 (2023) 25468–25482.
[26] S. Li, Y. Wang, X. Wang, et al., ACS Nano 17 (2023) 22399–22409.
[27] Q. Cheng, S. Li, Y. Ma, et al., Chin. Chem. Lett. 31 (2020) 1235–1238.
[28] G. Sun, M. Zuo, Z. Xu, et al., ACS Appl. Bio. Mater. 5 (2022) 3320–3328.
[29] R.J. Hooley, S.R. Shenoy, J. Rebek Jr., Org. Lett. 10 (2008) 5397–5400.
[30] Y. Liang, M. Zhu, T. Xu, et al., Molecules 28 (2023) 5715.
[31] J. Xing, Q. Gong, R. Zou, et al., Chin. Chem. Lett. 34 (2023) 107786.
[32] G.V. Smirnova, O.N. Oktyabrsky, Biochemistry 70 (2005) 1199–1211.
[33] M.B. Hillyer, C.L.D. Gibb, P. Sokkalingam, et al., Org. Lett. 18 (2016) 4048–4051.
[34] F.U. Rahman, H.N. Feng, Y. Yu, Org. Chem. Front. 6 (2019) 998–1001.
[35] X. Tian, M. Zuo, P. Niu, et al., ACS Appl. Mater. Interfaces 13 (2021) 37466–37474.
[36] P. Koprowski, A. Kubalski, Pflugers Arch. 438 (1999) 361–364.